

---

# Unsupervised Learning by Deep Scattering Contractions

---

Mia Xu Chen<sup>1,2</sup>, Xiuyuan Cheng<sup>2</sup>, and Stéphane Mallat<sup>2</sup>

<sup>1</sup>Dept. of Electrical Engineering, Princeton University, NJ, USA

<sup>2</sup>Depart. d'Informatique, École Normale Supérieure, Paris, France

xuchen@princeton.edu, xiuyuan.cheng@ens.fr, mallat@di.ens.fr

## Abstract

We introduce a deep scattering network, which computes invariants with iterated contractions adapted to training data. It defines a deep convolution network model, whose contraction properties can be analyzed mathematically. A cascade of wavelet transform convolutions are computed with a multirate filter bank, and adapted with permutations. Unsupervised learning of permutations optimize the contraction directions, by maximizing the average discriminability of training data. For Haar wavelets, it is solved with a polynomial complexity pairing algorithm. Translation and rotation invariance learning is shown with classification experiments on hand-written digits.

## 1 Introduction

The curse of high-dimensional learning results from the huge space volume. A uniform sampling requires a number of examples which increases exponentially with the dimension. Scattering transforms reduce the space volume by iteratively applying contractive operators, with a deep convolution network architecture [2, 5]. These contractions compute invariants and progressively decrease the space dimension to circumvent the curse of dimensionality. We introduce a deep scattering architecture implemented with a standard multirate filter bank, where learning is introduced with permutation operators. It rotates the space with orthogonal wavelet transforms and implements directional contractions with modulus operators. It provides a simple deep convolution network model, whose properties can be analyzed mathematically, because filter coefficients do not need to be modified.

Section 2 begins by introducing scattering transforms with a non-linear multirate filter bank. It computes wavelet transform convolutions and modulus non-linearities. Section 3 describes adapted scattering transforms, which optimize contraction directions with permutations. For Haar wavelets, it amounts to a pair matching problem, as explained in Section 4, which yields hierarchical invariants over multiscale groups. The scattering transform is then calculated with a cascade of additions and subtractions over pairs of points.

By adapting contractions with simple operators, a goal of this paper is to highlight important principles which govern the structure of deep convolution networks, and relate them to standard signal processing tools. Contractions are potentially dangerous because they can strongly reduce distance along certain directions and hence the discriminability of elements in different classes. Supervised data provides information to evaluate distances across classes, and thus adapt contractions to avoid reducing them too much.

---

The authors' names are in alphabetical order.

This work was supported by the ERC grant InvariantClass 320959.

Unsupervised learning can only implement weaker contraction criteria on training samples. We show that such optimizations amounts to computing sparse signal representations, similarly to sparse auto-encoders [4]. These results are illustrated by numerical experiments on modified MNIST digit images in Section 5. It shows that unsupervised scattering networks can learn translation and rotation invariant descriptors, with no prior information.

## 2 Scattering Transforms

A scattering transform is computed with a cascade of wavelet transforms and modulus non-linearities [2]. We reintroduce this transformation as a product of multirate filter bank operators, which is closer to deep convolution networks [5], and allows to generalize it for learning.

### 2.1 Modulus Filter-Bank

A multirate filter bank computes convolutions of  $x \in \mathbb{R}^d$  with a low-pass filter  $h$  and a high-pass filter  $g$ , and subsamples the output by a factor 2:

$$Hx(n) = x \star h(2n) \text{ and } Gx(n) = x \star g(2n) .$$

To avoid boundary issues, we consider  $x$  as a  $d$ -periodic signal, where  $d$  is a power of 2. The low-pass filter  $h$  is real but  $g$  may be complex valued. Both filters have a finite impulse response of size  $K$ . We write  $Wx = (Hx, Gx)$  the resulting multirate filtering. In the following, we shall impose that

$$\forall x \in \mathbb{R}^d, \quad \|Wx\|^2 = \|Hx\|^2 + \|Gx\|^2 = \|x\|^2 .$$

A fast wavelet transform iteratively applies  $W$  to the low-pass output  $Hx$ , as illustrated in Figure 1(a). The resulting orthogonal wavelet transform at the scale  $2^J$  is

$$\mathbf{W}_J x = (H^J x, GH^j x)_{0 \leq j < J} .$$

The first component is the averaged signal

$$H^J x = x \star \phi_J(2^J n),$$

where  $\phi_J$  is a low-pass filter of support  $K2^J$ . The wavelet coefficients are

$$GH^j x = x \star \psi_j(2^j n),$$

where  $\psi_j$  is a dilated band-pass filter whose support is of size  $K2^j$ .

Complex nearly analytic wavelet transforms are implemented with a nearly analytic complex filters  $g$ . It however requires to slightly modify the filter bank by first extending the dimension of  $x$  from  $d$  to  $2d$  with a linear interpolation [6]. Real orthogonal wavelet transforms are implemented with real conjugate mirror filters  $(h, g)$  which satisfy

$$|\hat{h}(\omega)|^2 + |\hat{h}(\omega + \pi)|^2 = 2 \text{ with } \hat{h}(0) = \sum_n h(n) = \sqrt{2}. \quad (1)$$

The high pass filter is  $g(n) = (-1)^n h(1-n)$ , and  $\sum_n g(n) = 0$ . One can prove that  $W = (H, G)$  is then an orthogonal operator in  $\mathbb{R}^d$  and that  $\{\phi_J(n - k2^J), \psi_j(n - k2^j)\}_{0 \leq k \leq d2^{-j}}$  is a wavelet orthonormal basis of  $\mathbb{R}^d$  [1].

Haar filters are simple examples defined by  $h(n) = 2^{-1/2}(\delta(n) + \delta(n-1))$  and  $g(n) = 2^{-1/2}(\delta(n) - \delta(n-1))$ . The resulting Haar scaling filter is  $\phi_J = 2^{-J/2}1_{[0, 2^J-1]}$  and the Haar wavelet is  $\psi_j = 2^{-j/2}(1_{[0, 2^j-1]} - 1_{[2^{j-1}, 2^j-1]})$ .

A modulus filter bank inserts a contraction with a modulus operator applied to the high frequency component  $Gx$  of  $x$ :

$$|G|x(n) = |x \star g(2n)| .$$

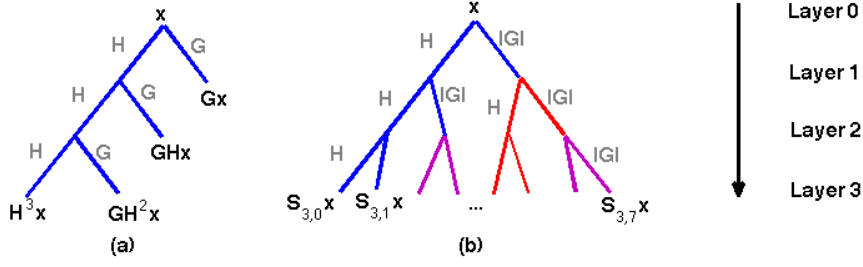


Figure 1: (a): A wavelet transform  $\mathbf{W}_J$  iteratively applies low-pass and high-pass filtering and subsampling operators  $H$  and  $G$ . A wavelet modulus  $|\mathbf{W}_J|$  applies a modulus on each output of  $G$ . (b): A scattering transform at scale  $2^J$  is a full modulus filter bank tree of depth  $J$ , which computes  $J$  layers of a deep network. For  $J = 3$ , it is a succession of wavelet transform subtrees  $|\mathbf{W}_j|$  for  $3 \geq j \geq 1$ , shown in blue, red and violet respectively.

Suppressing the phase or the sign performs a non-linear demodulation which shifts part of the signal energy towards the lower frequencies. This modulus is not applied to  $Hx$  which is already a low frequency signal. With an abuse of notation, we denote by  $|x|$  the vector obtained by applying the entry-wise modulus operator to a vector  $x \in \mathbb{R}^d$ , that is,  $|x| = \{|x(n)|\}_{1 \leq n \leq d}$ , and we write  $|W|x = (Hx, |G|x)$ . If  $x$  is real positive, which is the case in a scattering cascade, then  $Hx$  is positive real so  $Hx = |Hx|$ . It is thus as if the modulus was also applied to  $Hx$ .

A modulus is contractive in the sense that  $||a| - |b|| \leq |a - b|$ , for any  $(a, b) \in \mathbb{C}^2$ . Since  $\|Wx - Wx'\| = \|x - x'\|$ , it results that  $|W|$  is contractive

$$\| |W|x - |W|x' \| \leq \|x - x'\|,$$

and it preserves the norm  $\| |W|x \| = \|x\|$ . It is important to realize that a modulus strongly contracts the signal space. Indeed,  $Gx$  is an oscillatory signal whose sign or phase changes rapidly. For real signals, a modulus reduces by 2 the range of variation of its coefficients.

## 2.2 Scattering as Iterated Wavelet Transforms

The scattering transform of  $x \in \mathbb{R}^d$  is defined by a product of modulus filtering operators:

$$S_J x = |W|^J x \in \mathbb{R}^d. \quad (2)$$

Since  $|W|$  is contractive and preserves the norm, it results that  $S_J = |W|^J$  is also contractive and preserves the norm:

$$\|S_J x - S_J x'\| \leq \|x - x'\| \text{ and } \|S_J x\| = \|x\|. \quad (3)$$

The operator product (2) iteratively computes  $S_j x = |W|S_{j-1}x$  for  $1 \leq j \leq J$ , with  $S_0 x = x$ . Each time,  $|W|$  splits  $S_{j-1}x$  in two vectors  $(HS_{j-1}x, |GS_{j-1}x|)$ . It results that  $S_j x$  is a concatenation of  $2^j$  vectors  $\{S_{j,k}x\}_{0 \leq k < 2^j}$  of dimension  $2^{-j}d$  each, with

$$S_{j,2k}x = HS_{j-1,k}x \text{ and } S_{j,2k+1}x = |GS_{j-1,k}x|. \quad (4)$$

This tree subdecomposition is illustrated in Figure 1(b). Each  $S_{j,k}$  can thus be written a product of  $2^j$  operators equal to  $H$  or  $|G|$ . Since  $h$  and  $g$  have a size  $K$ , the scattering operator  $S_J$  has a support of size  $K2^J$ . Each  $S_J x(n)$  is computed from  $K2^J$  consecutive values of  $x$ . If we suppress the modulus non-linearity and replace  $|G|$  by  $G$  then  $S_J$  has totally different properties. It is then a linear wavelet packet orthogonal transform introduced in [7].

A scattering operator is implemented as a product of multirate filtering modulus, but its properties depend upon the underlying wavelet transform. A wavelet transform modulus at the scale  $2^l$  is defined by

$$|\mathbf{W}_l|x = (H^l x, |G|H^j x)_{0 \leq j < l}.$$

$m$	1	2	3	4	5
$\sigma_m^2$	1.8	1.4	$5.8 \times 10^{-1}$	$1.2 \times 10^{-1}$	$1.2 \times 10^{-2}$

Table 1: Value of the total variance  $\sigma_m^2$  of all scattering coefficients of order  $m$  as a function of  $m$ , for a Gaussian white noise random vector.

The modulus is applied only to the output of  $G$ :

$$|G|H^j x = |x \star \psi_j(2^j n)|.$$

The modulus suppresses the wavelet transform phase and hence computes an envelop which is approximately invariant to translations smaller than  $2^j$ .

A scattering transform  $S_J$  can be factorized as a product of wavelet transform modulus:

$$S_J = |\mathbf{W}_1| \dots |\mathbf{W}_{J-1}| |\mathbf{W}_J|.$$

Indeed, for each  $0 \leq k < 2^J$  there exists  $0 \leq m(k) \leq J$  such that

$$S_{J,k} = H^{J-\sum_l j_l} \prod_{l=1}^{m(k)} |G|H^{j_l} \text{ with } \sum_l j_l \leq J.$$

Each  $|G|H^{j_l}$  is calculated by the wavelet transform modulus  $|\mathbf{W}_{j_l}|$ . Figure 1(b) illustrates the factorization of the scattering operator  $S_J$  into the modulus of wavelet transforms  $|\mathbf{W}_{j_l}|$ , for  $J = 3$ .

The index  $m(k)$  is the number of times that  $|G|$  appears in the calculation of  $S_{J,k}$ . There are  $\binom{J}{m}$  vectors  $S_{J,k}$  of order  $m$ . Since the contraction is produced by  $|G|$ , the index  $m$  can be interpreted as a contraction factor. It plays an essential role to analyze the properties of these deep network coefficients. For a random vector  $X$  in  $\mathbb{R}^d$ , we define  $\sigma_m^2 = \sum_{k, m(k)=m} \text{Var}(S_{J,k}X)$  as the total variance of all coefficients of order  $m$ . Each modulus is applied to the output of a filter  $G$  which produces a zero-mean random vector. It thus strongly reduces the variance, and  $\sigma_m^2$  typically decreases exponentially with  $m$ . Table 1 gives its value for a Gaussian white random vector, which is an average measure of volume reduction in the signal space. One can show that  $\sigma_m^2 \approx (1 - \frac{2}{\pi})^m \cdot \binom{J}{m}$ , which is verified numerically in Table 1. Beyond  $m = 4$  the variance of coefficients becomes negligible and the corresponding scattering coefficients thus carry little information. Eliminating coefficients of order  $m > 4$  reduces the number of scattering coefficients from  $d$  to about  $(\log_2^4 d)/24$ .

### 3 Adapted Scattering

Scattering transforms are computed by deep convolution network, where the network weights are specified by the filters  $h$  and  $g$ . Learning network weights in convolution networks can thus be interpreted as a filter adaptation. As long as  $h$  remains an averaging filter and  $g$  is a high pass filter, modifying the filter values has marginal effects. Cascading such subsampled filtering still defines a wavelet transform. The number of vanishing moments or the wavelet regularity may be modified [1], but it does not modify much the wavelet coefficient properties. Major modifications of wavelet coefficients are however obtained by modifying the orbit (ordering of coefficients) along which convolutions are performed. For example, rotation invariant scattering transforms are calculated by also computing convolutions along rotation parameters in a deep scattering network [8]. This suggests to adapt wavelet transforms with permutations of the network variables before applying convolution operators. Let  $\pi$  be a permutation of  $\{1, \dots, d\}$ . It acts on  $x \in \mathbb{R}^d$  as a linear orthogonal operator, written  $z = \pi x \in \mathbb{R}^d$ , with  $z(n) = x(\pi(n))$ .

An adapted scattering inserts a permutation  $\pi_j$  of  $\{1, \dots, d\}$ , before each multirate modulus convolution:

$$S_j x = |W| \pi_j S_{j-1} x,$$

where  $\pi_j$  makes a permutation of the  $d$  coordinates of  $S_{j-1}x$  before applying  $|W|$ . It results that

$$S_J = |W| \pi_J \dots |W| \pi_2 |W| \pi_1 .$$

Since each  $\pi_j$  is a linear orthogonal operator,  $S_J$  remains contractive and preserves the signal norm:

$$\|S_J x - S_J x'\| \leq \|x - x'\| \text{ and } \|S_J x\| = \|x\| . \quad (5)$$

Geometrically,  $W\pi_j$  is a rotation of the signal space. It depends on  $\pi_j$ , which thus modifies the “directions” in which the modulus contractions are acting. The group of permutations is a group of rotations among which we shall search for particular rotations which optimize the contraction directions for learning. Optimizing permutations are typically  $NP$ -hard problems. However, the problem is not as bad as it seems because  $|W|$  computes convolutions with filters  $h$  and  $g$  of small support  $K$ . The output values thus depend on local ordering properties. For Haar filters, Section 4.1 shows that the ordering reduces to a pairing problem.

A scattering  $S_J$  operators is not invertible because the modulus loses a complex phase or a sign. In the real case, for almost all pairs of unitary operators  $(A, B)$  it has been proved [11] that the operator  $(|A|, |B|)$  is invertible on  $\mathbb{R}^d$ . If  $W$  is real, one can thus expect that  $(|W\pi^0|, |W\pi^1|)$  are invertible for “sufficiently different” permutations  $\pi^0$  and  $\pi^1$ . A necessary and sufficient condition is given on  $\pi^0$  and  $\pi^1$  for this result to hold for a Haar filtering.

### 3.1 Adapted Haar Scattering

A Haar modulus filtering computes

$$Hx(n) = \frac{x(2n) + x(2n+1)}{\sqrt{2}} \text{ and } |G|x(n) = \frac{|x(2n) - x(2n+1)|}{\sqrt{2}} .$$

Observe that  $(Hx(n), |G|x(n))$  is a permutation invariant representation of  $(x(2n), x(2n+1))$ , which specifies the two values of  $x(2n)$  and  $x(2n+1)$  because

$$\max(x(2n), x(2n+1)) = \frac{Hx(n) + |G|x(n)}{\sqrt{2}} \text{ and } \min(x(2n), x(2n+1)) = \frac{Hx(n) - |G|x(n)}{\sqrt{2}} .$$

An adapted Haar scattering is thus a cascade of permutation invariant operators over matched pairs.

We say that two permutations  $\pi^0$  and  $\pi^1$  are “interlacing” if there exists no strict subset  $\Omega$  of  $\{1, \dots, d\}$  such that  $\pi^0$  and  $\pi^1$  are pairing elements within  $\Omega$ . The following theorem derives a condition to recover a signal from  $2^J$  vectors of invariant Haar scattering coefficients.

**Theorem 3.1.** *Suppose that  $x \in \mathbb{R}^d$  takes more than 2 different values.*

- (1) *If  $W$  is a Haar filtering, then  $(|W|\pi^0, |W|\pi^1)$  is invertible if  $\pi^0$  and  $\pi^1$  are interlacing.*
- (2) *If  $\pi^0$  and  $\pi^1$  are interlacing then any  $x \in \mathbb{R}^d$  can be recovered from the  $2^J$  scattering transforms  $S_J x$  computed from the  $2^J$  families of permutations  $(\pi_1^{\epsilon_1}, \dots, \pi_J^{\epsilon_J})$  defined by all binary vectors  $(\epsilon_1, \dots, \epsilon_J)$  with  $\epsilon_j \in \{0, 1\}$ .*

*Proof.* Property (2) is proved by applying (1) recursively to  $(|W|\pi^0 S_j x, |W|\pi^1 S_j x)$  for  $J-1 \geq j \geq 0$ .

To prove (1), notice that if  $n_1, n_2, n_3$  is a triplet where  $(n_1, n_2)$  is a pair in  $\pi^0$  and  $(n_1, n_3)$  a pair in  $\pi^1$  then the values  $x(n_1), x(n_2), x(n_3)$  are uniquely determined from  $(|W|\pi^0 x, |W|\pi^1 x)$ , unless  $x(n_1) \neq x(n_2)$  and  $x(n_2) = x(n_3)$ . The interlacing condition implies that  $\pi^1$  pairs  $n_2$  to an index  $n_4$  which can not be  $n_3$  or  $n_1$ . Moreover, the four values of  $x(n_1), x(n_2), x(n_3), x(n_4)$  are specified unless  $x(n_4) = x(n_1) \neq x(n_2) = x(n_3)$ . This interlacing argument can be used to extend to  $\{1, \dots, d\}$  the set of all indices  $n_i$  for which  $x(n_i)$  is specified, unless  $x$  takes only two values. If that is not the case then  $x$  can be recovered, which proves the theorem.  $\square$

## 4 Unsupervised Learning

Learning a scattering metric amounts to finding the most appropriate directions along which to contract the space, and hence optimize permutations. For Haar wavelets, we show that this optimization can be reduced to pairing problems. We then concentrate on unsupervised learning.

### 4.1 Haar Pairing

To a permutation  $\pi$ , we associate a pairing  $p_\pi$  defined by the unordered set of  $d/2$  pairs  $\{(\pi(2n), \pi(2n+1))\}_{n \leq d/2}$ . Many permutations  $\pi^0$  and  $\pi^1$  have the same pairing  $p_{\pi^0} = p_{\pi^1}$ . A Haar scattering metric is only specified by these pairing operators. Indeed, if  $p_{\pi_j^0} = p_{\pi_j^1}$  for  $1 \leq j \leq J$  then one can verify by induction on  $J$  that there exists a permutation  $\pi$  such that  $S_J^0 = |W| \pi_J^0 x_J \dots |W| \pi_1^0$  and  $S_J^1 = |W| \pi_J^1 \dots |W| \pi_1^1$  satisfy  $S_J^0 = \pi S_J^1$ . It results that the scattering metrics are identical:

$$\forall (x, x') \in \mathbb{R}^{2d}, \quad \|S_J^0 x - S_J^0 x'\| = \|S_J^1 x - S_J^1 x'\|.$$

The optimization of a Haar scattering metric is reduced to an optimization of pairing operators. Ordering problems are typically *NP*-hard, but not pairing problems. If  $C(p_\pi)$  is an additive cost of each pair

$$C(p_\pi) = \sum_{n=1}^{d/2} c(\pi(2n), \pi(2n+1)) \quad (6)$$

then  $p_{\pi^*} = \arg \min_{p_\pi} C(p_\pi)$  is computed with  $O(d^3)$  operations with the Blossom Algorithm of Edmonds [9]. Computations in this paper use the implementation in [10]. The next section explains how to construct such additive costs for unsupervised learning.

### 4.2 Unsupervised Contraction Learning

A contraction can reduce too much the distance between two points which do not belong to the same class, and thus strongly reduce their discriminability. In general, this can not be fully avoided with unsupervised data. However, one can optimize contractions by maximizing the average distance between training samples, so that this loss of discriminability becomes less likely. We show that it implies computing sparse signal representations.

A scattering progressively contracts the scattering metric  $\|S_{j-1}x - S_{j-1}x'\|$ , by applying  $|W|\pi_j$  for  $1 \leq j \leq J$ . We consider unlabeled examples as realizations of a random vector  $X \in \mathbb{R}^d$ , which is an unknown mixture of different classes. The operator  $|W|\pi_j$  strongly contracts the signal space but it should reduce as little as possible the average Euclidean distance between realizations of  $S_{j-1}X$ , to avoid confusing elements of different unknown classes. We thus want to maximize the variance  $\sigma^2(S_j X)$  of  $S_j X$ . Since  $\sigma^2(S_j X) = \mathbb{E}\|S_j X\|^2 - \|\mathbb{E}(S_j X)\|^2$  and  $\mathbb{E}\|S_j X\|^2 = \mathbb{E}\|S_{j-1}X\|^2$ , this is equivalent to finding a permutation  $\pi_j$  which minimizes

$$\|\mathbb{E}(S_j X)\|^2 = \|\mathbb{E}(|W|\pi_j S_{j-1}X)\|^2.$$

From  $q$  realizations  $\{x_i\}_{i \leq q}$ , we estimate  $\|\mathbb{E}(S_j X)\|$  with the empirical sum  $\|\sum_{i=1}^q S_j x_i\|$ . It is a mixed  $\mathbf{l}^1$  norm along realizations  $x_i$  and an  $\mathbf{l}^2$  norm across the scattering coordinates. This is a sparsity norm which is optimized so that  $W\pi_j S_{j-1}X$  has a sparse representation. Sparsity appears in this optimization because the distance between two vectors having many zero coordinates is not much reduced by applying a modulus on the coordinate of these vectors. Indeed,  $||a| - |b|| = |a - b|$  if  $a$  or  $b$  is zero. The mixed  $\mathbf{l}^2$  and  $\mathbf{l}^1$  norm can also be replaced by a simpler  $\mathbf{l}^1$  sparsity norm.

For a Haar scattering transform, the sparsity norm is an additive cost on the pairing  $p_{\pi_j}$ :

$$\left\| \sum_{i=1}^q S_j x_i \right\|^2 = C(p_{\pi_j}) = \sum_{p=1}^{d/2} c(\pi_j(2p), \pi_j(2p+1)),$$

with

$$c(k, k') = \left( \sum_{i=1}^q S_{j-1}x_i(k) + S_{j-1}x(k') \right)^2 + \left( \sum_{i=1}^q |S_{j-1}x_i(k) - S_{j-1}x(k')| \right)^2.$$

It is solved with the Blossom algorithm with  $O(d^3)$  operations. The unsupervised learning algorithm iteratively computes an optimized pairing  $p_{\pi_j}$  for  $j$  going from 1 to  $J$ . One can also impose constraints on the pairing to reduce computations and incorporate some prior information. An inner-node pairing in the filter bank tree imposes that  $\pi_j$  pairs coefficients within each vector  $S_{j,k}x$ , and performs the same pairing for all  $0 \leq k < 2^j$ .

There is typically not a unique pairing which minimizes the unsupervised contraction cost. Let us consider for example a random vector  $X$  which is stationary and has a period  $d$ . Any translation of the pairing yields the same cost because of the stationarity. These pairing being equally valid, one can reduce the classification variance by using them all. We thus use a bagging algorithm which estimates several ordered scattering from several training sets, and aggregates these multiple scattering vectors to compute a linear SVM classification.

## 5 Numerical Experiments

Unsupervised contraction learning does not differentiate subclasses and can thus mostly learn sources of variability which are in common for most of the classes. Geometric variability such as translations, rotations or deformations are such examples. The MNIST digit recognition data bases provides a simple framework to study the learning of these sources of variability.

Learning of translations and deformations is evaluated in Section 5.1 on the original MNIST database, which has 60,000 training samples and 10,000 testing samples. A modified MNIST data basis with 3D digit rotations is studied in Section 5.2.

### 5.1 MNIST Digit Recognition

We consider a random permutation of the MNIST image pixels, illustrated in Figure 2a. Each image is thus considered as a non-ordered bag of pixels. These experiments tests several aspect of the algorithm: the ability to recover spatial neighborhood information and the classification accuracy without location information.

The permutation learning is first performed with inner-node pairing optimizations, which means that for each level  $j$ , the same pairing function is used to associate the coefficients of each  $S_{j,k}x$  for  $0 \leq k < 2^j$ . These pairings perform a multiscale estimation of relative spatial locations. We say that two coefficients  $S_{j,k}(n)$  and  $S_{j,k}(n')$  are spatially connected if they are computed with operators whose supports of size  $2^j$  are spatially connected in the original image domain. We only consider coefficients whose amplitude are non-negligible and thus play a role in the classification. Over the first three levels  $1 \leq j \leq 3$ , a 100% of the pairs are connected, which shows that all pairing are spatially connected. For  $j = 4$  and  $j = 5$  the proportion of connected pairs are respectively 85% and 67%. The connectivity ratio decreases with the scale because long range correlations are weaker and spatially non-connected pairs may become more similar than spatially connected ones.

MNIST images have  $d \leq 2^{10}$  pixels so scattering operators can be computed at scales  $2^J \leq 2^{10}$ . The classification error decreases when  $J$  increases and the best accuracy is obtained for  $J = 10$ , which corresponds to a maximally invariant representation. We compute  $N$  adapted scattering operators with unsupervised pairing over  $N$  different subsets of training samples. The  $N$  different scattering vectors  $S_Jx$  are aggregated and fed into a linear SVM. The energy of scattering coefficients decrease exponentially with  $m$ , as shown by Table 1 for a Gaussian process. Table 2b shows that best classification results are obtained by keeping only coefficients of order  $m \leq 4$ . Since  $2^J = d$ , we thus keep about  $(\log_2 d)^4 / 24$  scattering coefficients as opposed to  $d$ . These figures are computed with an aggregation of  $N = 10$

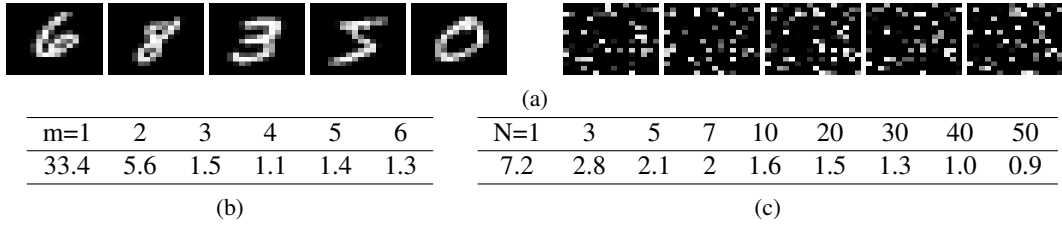


Figure 2: (a) Sample images from MNIST before and after permutation. (b) The classification error rate as a function of the scattering order  $m$ , when  $J=10$ . (c) The classification error rate as a function of the number of adapted scattering operators ( $N$ ), when  $J=10$ .

different scattering vectors, but the optimum for  $m = 4$  does not depend upon  $N$ . Table 2c gives the classification error rate as a function of  $N$ . The performance increases slowly for  $N \geq 10$ , and does not improve beyond  $N = 50$ , which is much smaller than  $2^J$ .

Almost all MNIST classification algorithms use prior information on the spatial location of pixels to build spatially localized descriptors, and deep convolution networks as well as translation invariant scattering transforms further use prior information on translation invariance. State of the art results, without making any modification of training vectors, is achieved by deep convolutional neural networks (0.53%, [5]), and scattering networks with Gabor wavelet (0.43% [2]). This unsupervised learning, uses no prior information on pixel location or on translation invariance. It reaches an error of 0.9% by optimizing inner-node pairing. If no constraint is imposed on the pairing algorithm, which may thus associates coefficients computed across different nodes in the filter bank tree, then the error increases to 1%. Indeed, for MNIST, intra-class variabilities are mostly due to translations and deformations. Appropriate invariants can be thus computed with inner-node pairing. Providing more flexibility increases the pairing variance, which explains the slight error increase. This flexibility can however produce useful invariants for non-translation invariants.

## 5.2 MNIST with 3D Rotations

To test the algorithm ability to build invariant to different source of geometric variability, we use the 3D rotated MNIST data basis constructed in [3]. Digit ‘9’ is removed from the data set as it is equivalent to the digit ‘6’ after rotation. Each digit is projected on a 3D sphere sampled over  $d = 4096$  points, and randomly rotated on the sphere, with a rotation variance  $\sigma^2 = 0.2$  [3].

Translations in the plane are now replaced by rotations over the sphere, on which one can not define convolution operators after sampling. The classification algorithms in [3] introduces an elegant solution which replaces convolution operators (diagonal in Fourier) by operators which are diagonal over the Laplacian eigenvectors on a graph. These algorithms use the 3D neighborhood of points on the sphere to define the graph connectivity. Table 2 gives the results reported in [3], with 19% error for a nearest neighbor algorithm, 5.6% for a two-layer fully connected neural network, and 6% for two best locally connected network algorithms. The adapted Haar scattering algorithm yields a smaller error of 2.2%, when computed at the maximum scale  $2^J = d$ , by aggregating  $N = 10$  scattering transforms, up the order  $m = 4$ . The Haar scattering thus reduces the error by an important factor although it uses no prior information on the 3D connectivity of points, which illustrates the learning abilities of this deep network structure.

Nearest Neighbors	Fully Connect.	Locally Connect. [3]	Spectral Net. [3]	Adapted Haar Scat.
19	5.6	6	6	<b>2.2</b>

Table 2: Percentage of errors on MNIST 3D rotation data set [3], with a nearest neighbor classifier, a fully connected two layer neural network, a locally connected network, a spectral network [3], and an adapted Haar scattering.



## References

- [1] S. Mallat, “A Wavelet Tour of Signal Processing: The Sparse Way”, Academic Press, 2009.
- [2] J. Bruna, S. Mallat, “Invariant Scattering Convolution Networks,” IEEE Trans. PAMI, 35(8): 1872-1886, 2013.
- [3] J. Bruna, W. Zaremba, A. Szlam, and Y. LeCun, “Spectral Networks and Deep Locally Connected Networks on Graphs,” ICLR 2014.
- [4] Y. Bengio, “Learning Deep Architectures for AI,” Foundations and Trends in Machine Learning, 2009.
- [5] Y. LeCun, K. Kavukvuoglu, and C. Farabet, “Convolutional Networks and Applications in Vision,” Proc. IEEE Int. Sump. Circuits and Systems 2010.
- [6] G. Selesnick, I. Baraniuk and Kingsbury, “A dual tree complex wavelet transform”, IEEE Signal Processing Magazine, no 123, 2005.
- [7] R. Coifman, Y. Meyer and M. Wickerhauser, “Wavelet analysis and signal processing”, in Wavelets and Their Applications, Jones and Barlett, pp. 153-178, 1992.
- [8] L. Sifre and S. Mallat, “Rotation, Scaling and Deformation Invariant Scattering for Texture Discrimination,” CVPR 2013.
- [9] J. Edmonds. Paths, trees, and flowers. *Canadian Journal of Mathematics*, 1965.
- [10] E. Rothberg of H. Gabow’s, “An Efficient Implementation of Edmond’s Algorithm for Maximum Matching on Graphs.” *JACM*, **23**, 1976.
- [11] R. Balana, P. Casazza, and D. Edidinb, “On signal reconstruction without phase,” Applied and Computational Harmonic Analysis, 2006.